

## Article

# Multi-Material Metamaterial Topology Optimization to Minimize the Compliance and the Constraint of Weight: Application of Non-Pneumatic Tire Additive-Manufactured with PLA/TPU Polymers

Shokouh Dezianian  and Mohammad Azadi \* 

Faculty of Mechanical Engineering, Semnan University, Semnan 35131-19111, Iran

\* Correspondence: m\_azadi@semnan.ac.ir

**Abstract:** In non-pneumatic tires, metamaterial cells could replace the pneumatic part of the tire. In this research, to achieve a metamaterial cell suitable for a non-pneumatic tire with the objective function of increasing compressive strength and bending fatigue lifetime, an optimization was carried out for three types of geometries: a square plane, a rectangular plane, and the entire circumference of the tire, as well as three types of materials: polylactic acid (PLA), thermoplastic polyurethane (TPU), and void. The topology optimization was implemented by the MATLAB code in 2D mode. Finally, to check the quality of cell 3D printing and how the cells were connected, the optimal cell fabricated by the fused deposition modeling (FDM) method was evaluated using field-emission scanning electron microscopy (FE-SEM). The results showed that in the optimization of the square plane, the sample with the minimum remaining weight constraint equal to 40% was selected as the optimal case, while in the optimization of the rectangular plane and the entire circumference of tire, the sample with the minimum remaining weight constraint equal to 60% was selected as the optimal case. From checking the quality of 3D printing of multi-materials, it was concluded that the PLA and TPU materials were completely connected.



**Citation:** Dezianian, S.; Azadi, M. Multi-Material Metamaterial Topology Optimization to Minimize the Compliance and the Constraint of Weight: Application of Non-Pneumatic Tire Additive-Manufactured with PLA/TPU Polymers. *Polymers* **2023**, *15*, 1927. <https://doi.org/10.3390/polym15081927>

Academic Editor: Xavier Colom

Received: 22 March 2023

Revised: 15 April 2023

Accepted: 17 April 2023

Published: 18 April 2023



**Copyright:** © 2023 by the authors. Licensee MDPI, Basel, Switzerland. This article is an open access article distributed under the terms and conditions of the Creative Commons Attribution (CC BY) license (<https://creativecommons.org/licenses/by/4.0/>).

**Keywords:** multi-material; metamaterial; topology optimization; non-pneumatic tire; 3D printing

## 1. Introduction

As an engineering issue, optimization is basically divided into three topics: size optimization, shape optimization, and topology optimization. In size optimization, the variables are the dimensions of the structure such as thickness, surface, and volume. Shape optimization determines the shape of the structure boundaries. Topology optimization in discrete structures examines the number and optimal connection of members [1].

Researchers have recently realized that by taking inspiration from nature, cellular structures can be designed in such a way that they have novel characteristics [1]. In addition, with optimization methods, all types of cells with desired properties can be designed. So far, many cells have been discovered and designed, and are generally divided into four categories: foams, lattice, Triply Periodic Minimal Surfaces (TPMS) planes, and TPMS skeletons [2,3].

Metamaterials arise from the replication of cells next to each other [1,4]. Owing to the complex structure of metamaterials, 3D printers are used to produce them. For example, a type of metamaterial that twists under pressure has been produced with a 3D printer [5].

Among the applications of metamaterials is in car tires. Metamaterial cells replace the pneumatic part of the tire and create non-pneumatic tires. One of the advantages of these types of tire is eliminating the worry of a flat tire and the need to adjust the air pressure inside the tire. These tires are notable for the easy method of manufacturing [6]. In addition, non-pneumatic tires are more environmentally friendly due to lower raw material

usage in their production [7,8]. Bras and Cobert [9] investigated the environmental impact of the Tweel tire during its life cycle, through the possibility of making these tires with recyclable and reusable materials. They concluded that non-pneumatic tires help to reduce the serious problems of the environmental pollution caused by the indestructibility of traditional tires [9]. Furthermore, the discussion of the environmental impact perfectly matches with the new sustainable management and treatment actions for end-of-life tires, such as the end-of-waste directives in Europe and the USA [10] or the waste disposal and public cleansing law in Japan [11].

These tires also have other advantages such as reducing rolling resistance and thus reducing fuel consumption and emissions [6,7,12–14].

There have been many activities to investigate non-pneumatic tires. One of the tires that has been designed is the Tweel tire. This tire has been examined from different aspects. This includes the possibility of manufacturing them with 3D printers [15], checking the mechanical behavior by a dynamic finite element model [16], checking the three-point bending properties and simulating this test using the finite element method [17], the effects of cell thickness on vertical stiffness and maximum local stress in cells and their weight [18], the noise produced by Tweel tires [19], investigation into different parameters affecting rolling resistance [20] and prediction of pressure distribution in the cell of this tire [21].

The Tweel tire was also designed for use on the moon, which led to a new structure called TweelTM. This tire has also been examined from different aspects, including modeling and simulating the dynamic interaction between tire and sand [22], the interaction of the tire shear layer with sand [23], examining different patterns to find a cell with a high shear bending force bearing considering the strain energy distribution [24] and investigating the ribbed metamaterial shear layer and selecting the shear layer with a specific cell geometry with the best pressure distribution in the contact area [25].

The use of optimization methods for the design of metamaterial cells has also been investigated. Cells have been optimized for one or more materials. Tavakli [26] developed a multi-material optimization algorithm. Numerical results show that the proposed algorithm is very close to the discrete scheme or 0–1. Zhengtong et al. [27] proposed an optimization algorithm for a truss foundation. In this method, the optimization of the use of different materials is considered. Chen et al. [28] presented a multi-material topology optimization algorithm for cell design by reducing stress concentration. This metamaterial cell also had the property of a negative Poisson ratio.

Chung and Du [29] developed a topology optimization framework for the design of multi-material cellular structures. The resulting cellular structure is a thermal metamaterial that must be exposed to temperature changes. Mansouri et al. [30] compressed a multi-material cellular structure. The results show that the multi-material cellular structure had better compressive properties. These multi-material structures had flexibility and load-bearing characteristics. Gao et al. [31] proposed a topology fatigue optimization approach. In this method, stress, volume, and fatigue strength are considered limitations and minimum compliance is the objective function.

In other research, Gao et al. [32] proposed a design method for the design of three-material auxetic metamaterials using the isogeometric topology optimization (ITO) method. Huang and Li [33] developed an algorithm for designing new multi-material topology optimization. Li et al. [34] also investigated the optimization of the topology of auxetic cellular composites using the surface set method.

Nguyen et al. [35] presented an approach for unit cell design using isogeometric analysis and parametric surface adjustment. Vogiatzis et al. [36] proposed a surface set-based method for topology optimization of single-material and multi-material metamaterials with a negative Poisson ratio (NPR). Zhang et al. [37] presented a new bi-material cell design method for chiral auxetic metamaterials. Zheng et al. [38] systematically investigated several isotropic materials concerning the elastic modulus and Poisson ratio. In this research, a method of topology optimization and optimal design of cells was used.

According to the literature, the studies for the optimization of metamaterial cells were carried out with:

- different optimization methods [24,29–34],
- different materials (one to several materials) [23,26,27,36],
- different objective functions and constraints [25,28].

Consequently, the innovation of the current research is related to:

- the optimization of the metamaterial cell with three materials and its possible application in non-pneumatic tires,
- the production and the examination of how to connect materials and the quality of 3D printing.

## 2. Materials and Methods

### 2.1. Samples

The main goal of this research is to design a non-pneumatic tire with an optimization method consisting of several materials. Different forces are applied to the tire. However, in this research, the compressive force caused by the weight of the car and the passengers and the bending force caused by the friction between the tire and the road were considered. In this article, it was assumed that the tire was moving along a straight road. As a result, lateral force was omitted. In future articles the impact of lateral force could also be investigated. According to this hypothesis and a review of articles, the dimensions and amount of force on the tire were selected [12,13,15,16,18,21,23,39–58]. These forces and the dimensions of the tire in question are shown in Figure 1. The combined compressive and bending force was selected as 1 kN. Considering that the problem was two-dimensional (2D), a concentrated load was applied.

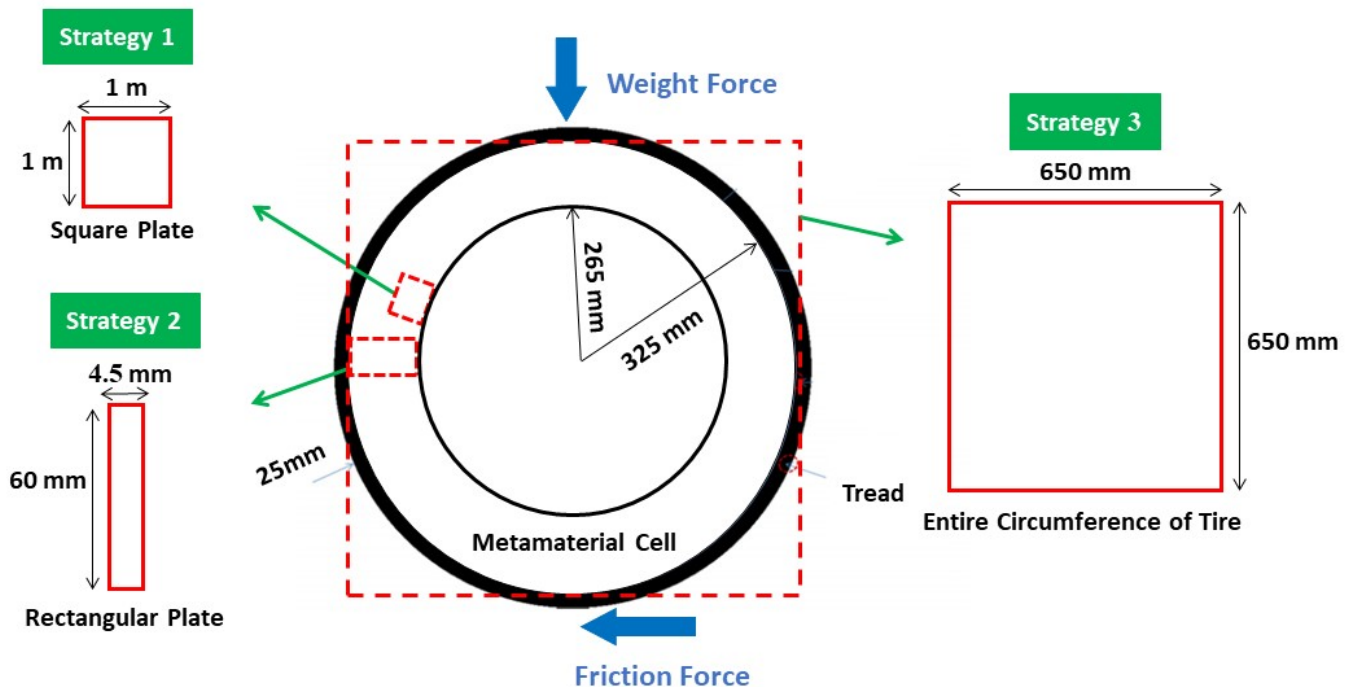


**Figure 1.** The dimensions of the tire plus the solution strategy.

To optimize the non-pneumatic tire, three types of solution methods were considered. In the first case (Strategy 1), a non-pneumatic tire was obtained by optimizing a square plane and putting together the optimized response in the pneumatic part of the tire (after optimization, this cell can be used in a scaled form in the tire). In the second case (Strategy 2), a rectangular plane was chosen equal to the height of the pneumatic tire section, which

was obtained by putting together the optimized response in the radial direction of the non-pneumatic tire. In the third mode (Strategy 3), optimization for the entire circumference of the tire was included.

## 2.2. Materials Specifications

In this research, to optimize and find a suitable cell to replace the pneumatic part of the tire, three types of materials including polylactic acid (PLA), thermoplastic polyurethane (TPU) and void were used. The producer of both types of polymeric filaments was the YS company. PLA is among the harder 3D printable polymers on the market. The Poisson ratio for this material is 0.36, its density is 1240 kg/m<sup>3</sup> [59], and its melting temperature is between 180 and 230 °C [60]. TPU polymers show properties such as toughness, strength, and wear resistance. The Poisson ratio of these materials is 0.3897, their melting temperature is 200–220 °C, and their density is 1200 kg/m<sup>3</sup> [61].

In the present article, the tensile properties of the materials, which have a more critical effect, were used. Tensile test samples were prepared according to the ISO-527 standard at a speed of 50 mm/min and fused deposition modeling (FDM) method with a repeatability of three tests with 3D printing parameters according to Table 1. In the 3D printer used, the extruder is moved by the belt system in the X-Y axes and the bed is moved by the lead screw in the Z axis. This printer is able to print parts with dimensions of 550 × 600 × 700 mm. It has an accuracy of 50 and 40 µm in the X-Y and Z axes, respectively. This device was designed and manufactured by the research laboratory of Advanced Materials Behavior (AMB) at the Faculty of Mechanical Engineering, Semnan University, Semnan, Iran. The results of the tensile test are shown in Table 2. These properties were used in the optimization.

**Table 1.** Parameters for 3D printing of PLA/TPU polymers.

Material	Speed (mm/s)	Nozzle Temperature (°C)	Infill (%)	Layer Height (mm)	Nozzle Diameter (mm)	Bed Temperature (°C)
PLA	20	180	100	0.2	0.2	25
TPU	20	220	100	0.2	0.2	25

**Table 2.** Mechanical properties of the materials studied.

Material	Yield Stress (MPa)	Elastic Modulus (MPa)
PLA	56.0 ± 2.5	3089.3 ± 100.7
TPU	4.1 ± 1.6	12.0 ± 0.6

## 2.3. Optimization Procedures

Metamaterials can be designed by using optimization processes. In these processes, optimization was performed for one cell, then by repeating and putting this cell together, a metamaterial structure was fabricated. Topology optimization was performed based on finite element analysis and sensitivity analysis. In each step, the properties of the elements were specified. Mathematical programming techniques were also used to obtain convergence of the response. More information is provided in Appendix A [62–68].

To perform optimization in the MATLAB software, the code written by Zuo and Saitou [69] was used. In this code, it is possible to optimize several materials in 2D mode. Therefore, the optimization of the three geometries in question was defined as shown in Figure 2. The parameters used in the optimization are also presented in Table 3.

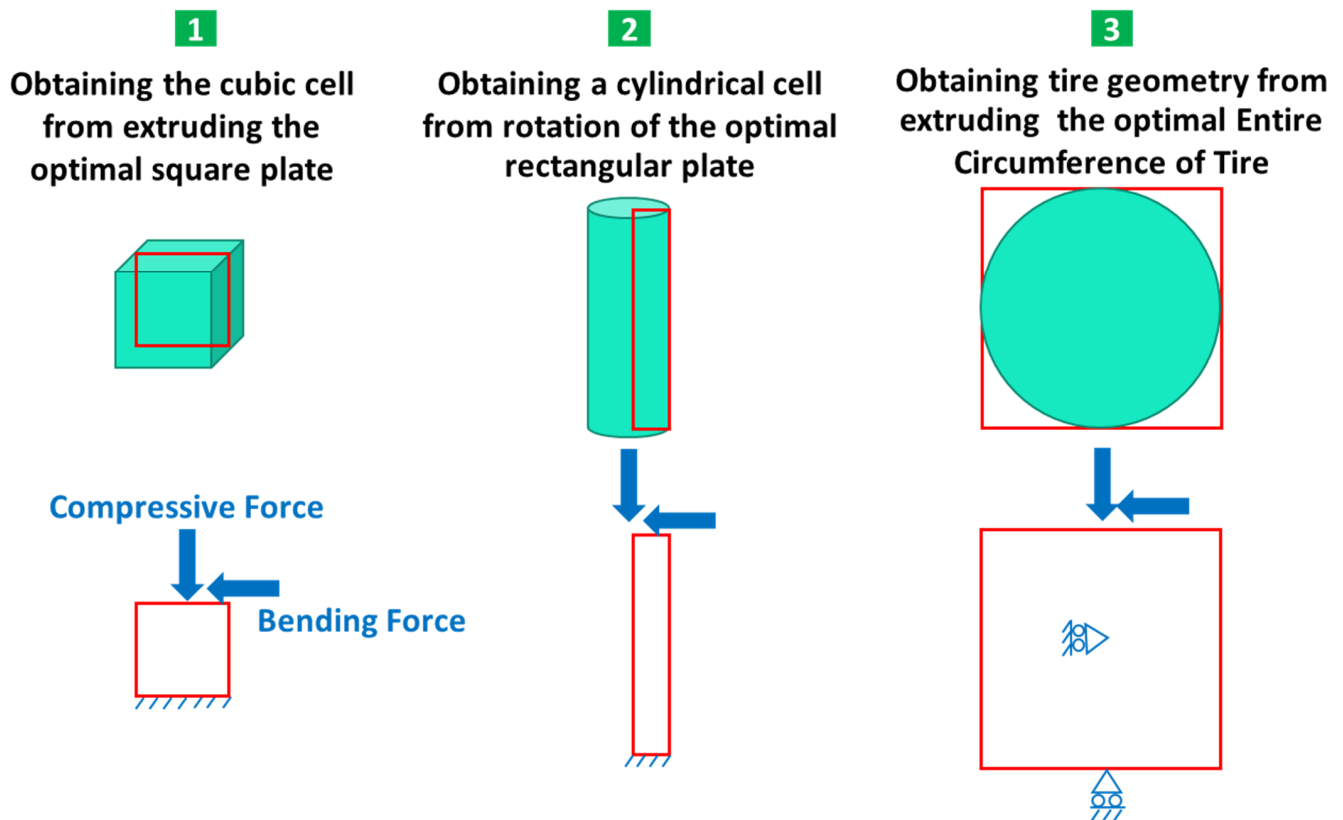


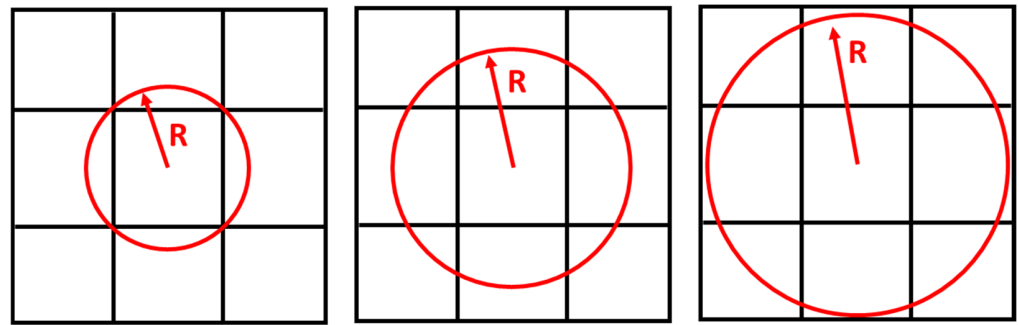
Figure 2. Problems defined in the MATLAB code.

Table 3. Optimization parameters in this research.

Objective	Constraint	R
Minimum Compliance	Remaining weight for 20, 40, and 60% of the total weight	1.2

One solution to prevent rasterization of the response is to use filters such as the neighborhood radius filter. In this filter, the color or density of each element is calculated as an average of the density of adjacent elements. The neighborhood radius is one of the optimization parameters. If there is a limitation in the construction method, a smaller neighborhood radius can be used. Moreover, if there is no limit to production, the neighborhood radius can be used more. In this case, the answer is more accurate. The neighborhood radius filter considers constructability in the optimization process. The larger the radius is, the more elements are involved. As a result, more elements have the same properties. If a smaller radius is used, the boundary between the void and the solid material is clearer. However, if this radius is too small, the elements will not be grouped. Figure 3 is presented for a better understanding of this method. For the optimization, the neighborhood radius filter with the symbol of R was used.

The code used contains two types of constraints: volume and price. However, in the present study, only the volume was used. To eliminate the effect of the price constraint, a value of 50% was considered. This means that both PLA and TPU materials should be used equally. The final answer should include 50% of the cheaper material and naturally 50% of the more expensive material. In addition, the normal vector related to the price of materials was defined as (1 1 1). This means that the price of all three: void, PLA and TPU, was assumed to be the same.



**Figure 3.** The radius filter to obtain a better objective.

To optimize the square plane, a  $1 \times 1$  m plane was selected, which was subjected to a compressive and bending force of 1 kN. By extruding the optimized 2D geometry, the desired cell was calculated. This cell is to be used in a scaled form in the tire. Similarly, for the optimization of the rectangular plane, a plane with dimensions of  $4.5 \times 60$  mm was selected, and the desired geometry was obtained from the rotation of this plane around the axis of symmetry (see Figure 1). This plane was also subjected to a compressive and bending force of 1 kN.

Optimizing the entire circumference of a tire with dimensions of  $650 \times 650$  mm was considered, and the desired result was obtained by extruding its optimized response to the width of the tire section. In the design of the tire, continuous contact between the tire and the road is very important for the safety of the car and its passengers. Therefore, a barrier was considered at the point of contact between the tire and the road to prevent the separation of these two. In addition, another restriction was also considered in the center of the tire to prevent the tire from sliding on the road.

In the MATLAB code used to investigate the effect of the length of the element on the optimization response, various analyses were performed, the results of which are shown in Figure 4. According to this figure, an element size of 25 mm was chosen.

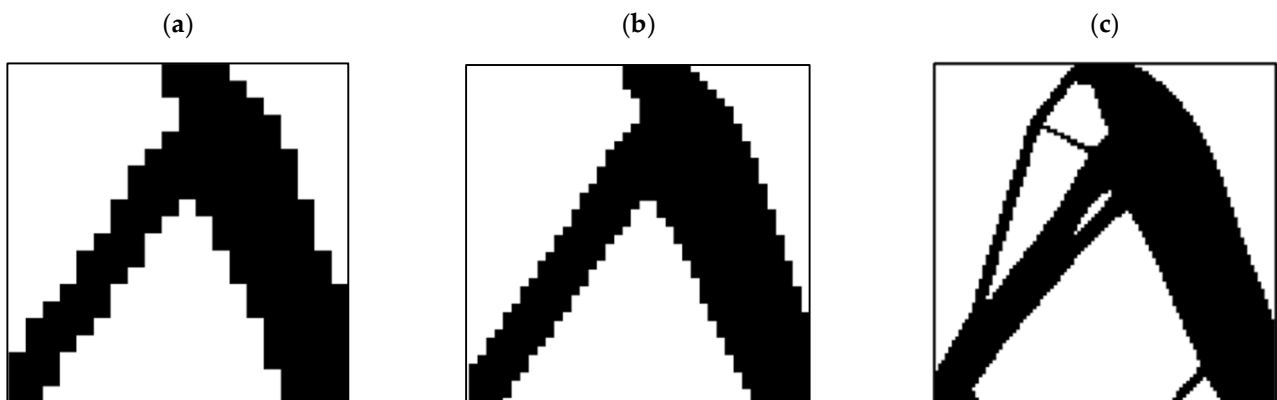


**Figure 4.** The effect of element size on the optimization response: (a) 50, (b) 25, and (c) 10 (mm).

#### 2.4. Printing Quality

To check the quality of 3D printing in the production of parts made of PLA and TPU and to check how to connect them, the optimal cell fabricated by the FDM method was observed using field emission scanning electron microscopy (FE-SEM) (Zeiss Sigma 300 HV, Jena, Germany). A gold coating was applied on the surface of the samples prior to SEM analysis.

### 3. Results and Discussion

#### 3.1. Outputs for Square Plane

A square plane with dimensions of  $1 \times 1$  m with an element length of 25 mm, which is equivalent to the number of 40 elements in each direction, was used for optimization with different volumes. Figure 5 illustrates the optimization results for various weight constraints. According to this figure, the sample with less remaining weight equal to 20% and 60% had discontinuity. This discontinuity requires support according to the manufacturing method (FDM), as in metamaterials it is very difficult, if not impossible, to separate these types of support from the main part due to the repetition of the cell and the complexity of the part. One of the ways to overcome this challenge is to use the constraint related to additive manufacturing. In this type of constraint, the overhang angle (the angle between the material and the horizontal line) is defined. In this case, angles greater than  $45^\circ$  that require support will not be fabricated along with the specimen. Therefore, the sample with a remaining weight of less than 40% was selected as the optimal sample.

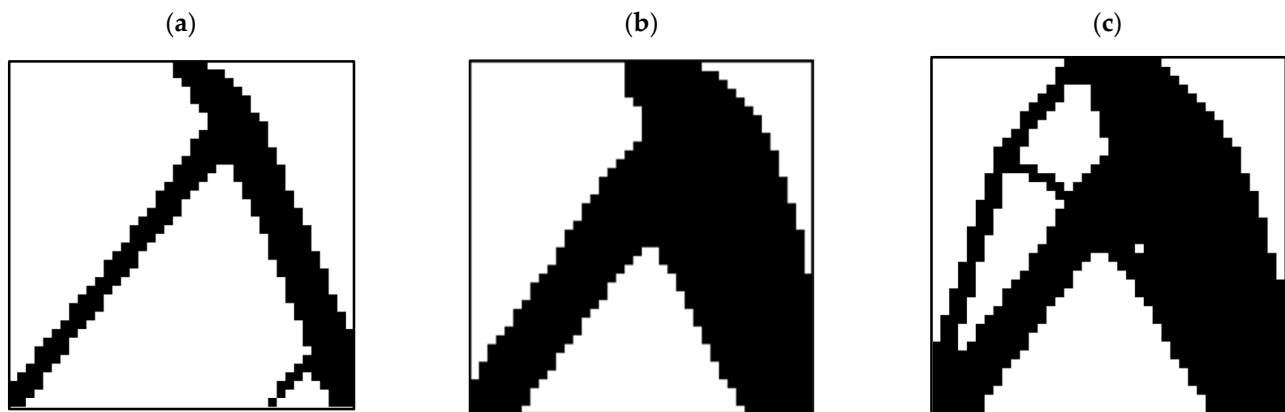


**Figure 5.** The response resulting from the optimization for the square plane in terms of (a) 20%, (b) 40%, and (c) 60% for the weight constraint.

This problem was implemented in a completely similar way in the ABAQUS software for both 2D and 3D modes. The problem defined in the ABAQUS software is shown in Figure 6. The answer obtained by the MATLAB code compared to the optimized cell with ABAQUS software is depicted in Figure 7.

According to Figure 7, where the quality of the optimization results is compared, the results are similar to each other to an acceptable extent. Therefore, the MATLAB code was used in 2D mode to optimize PLA and TPU materials along with voids in the target plane. Since the sample with 40% of the original weight was selected as the optimal sample in the optimization of the square plane, the same constraint was used in this step as well. As shown in Figure 7a, the weight of the sample in 3D mode (ABAQUS) was 486 g. while the weight of the solid sample was 1240 g. Therefore, it can be concluded that the remaining weight was about 40% of the solid weight specimen. The convergence diagram of the objective function is shown in Figure 8 and the result obtained is also depicted in Figure 9. According to the results, the answer obtained can only be implemented with the help of 3D printers with two nozzles.

The answer for the optimization of a square plate consisting of PLA and TPU materials was fabricated in two scales by the FDM 3D printer. The print parameters were considered according to Table 1. These cells are demonstrated in Figure 10.

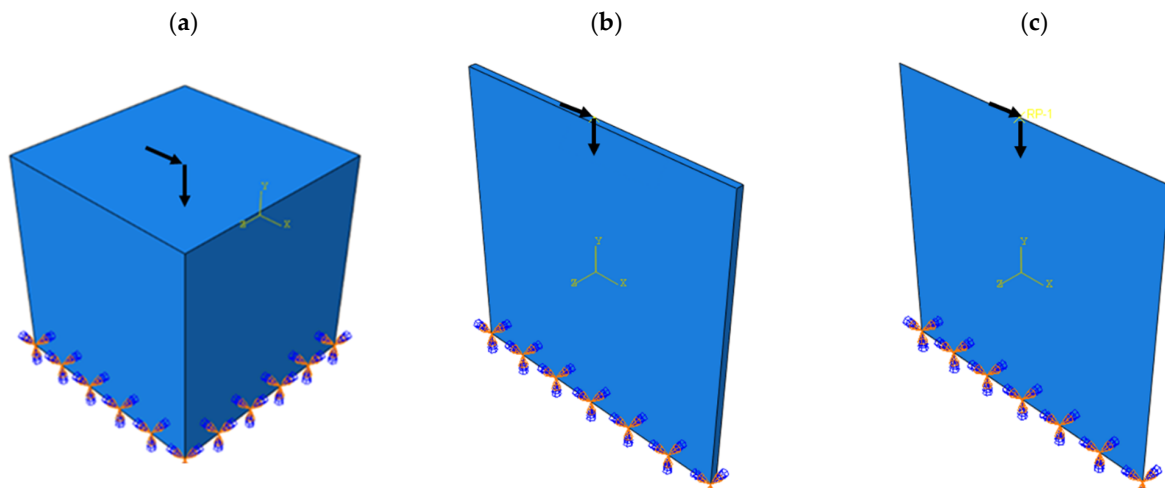


Figure 6. The problem defined in ABAQUS software: (a) 3D model, (b) 3D model with low thickness, and (c) 2D model.

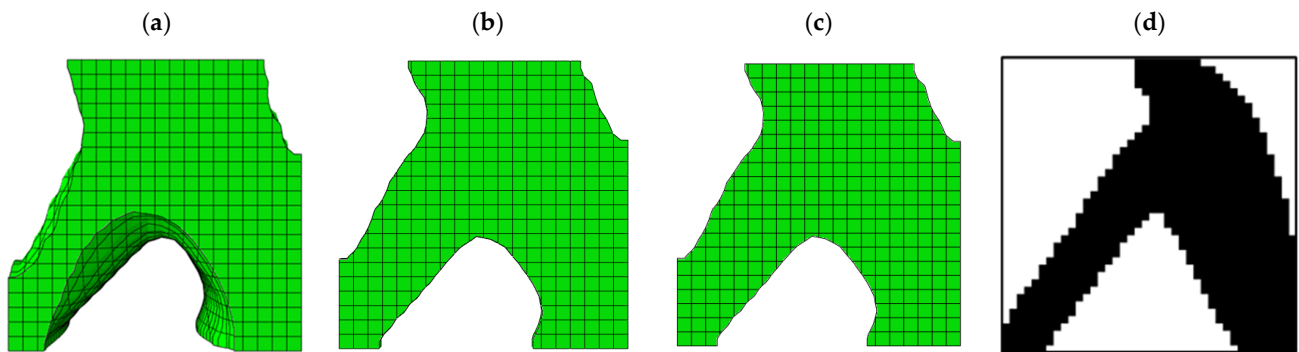


Figure 7. The comparison of the results obtained from ABAQUS software: (a) 3D model, (b) 3D model with low thickness, (c) 2D model, and (d) plus results of the MATLAB code.

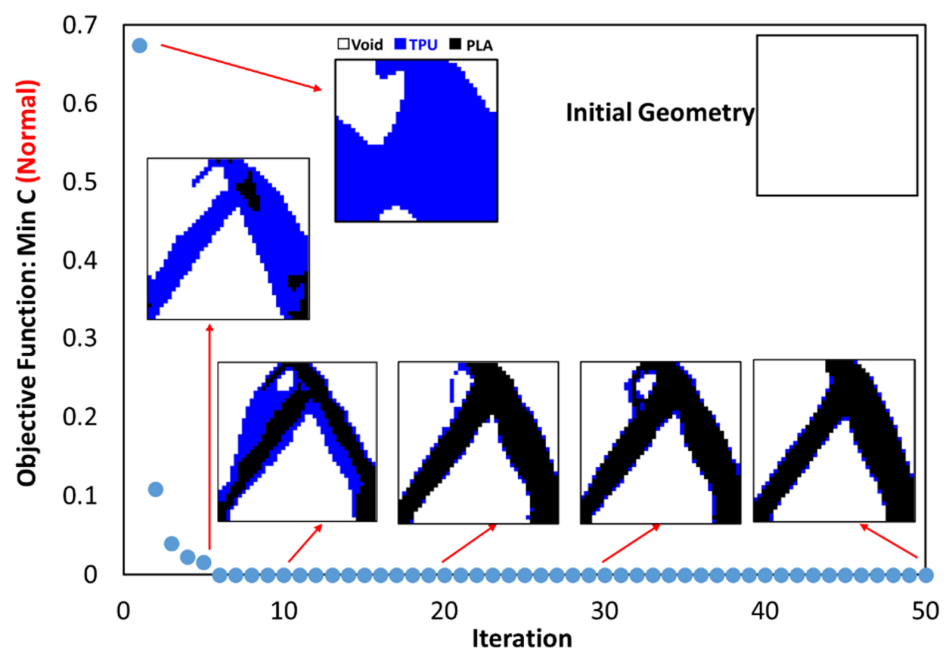


Figure 8. The convergence diagram of the objective function for optimal material distribution.

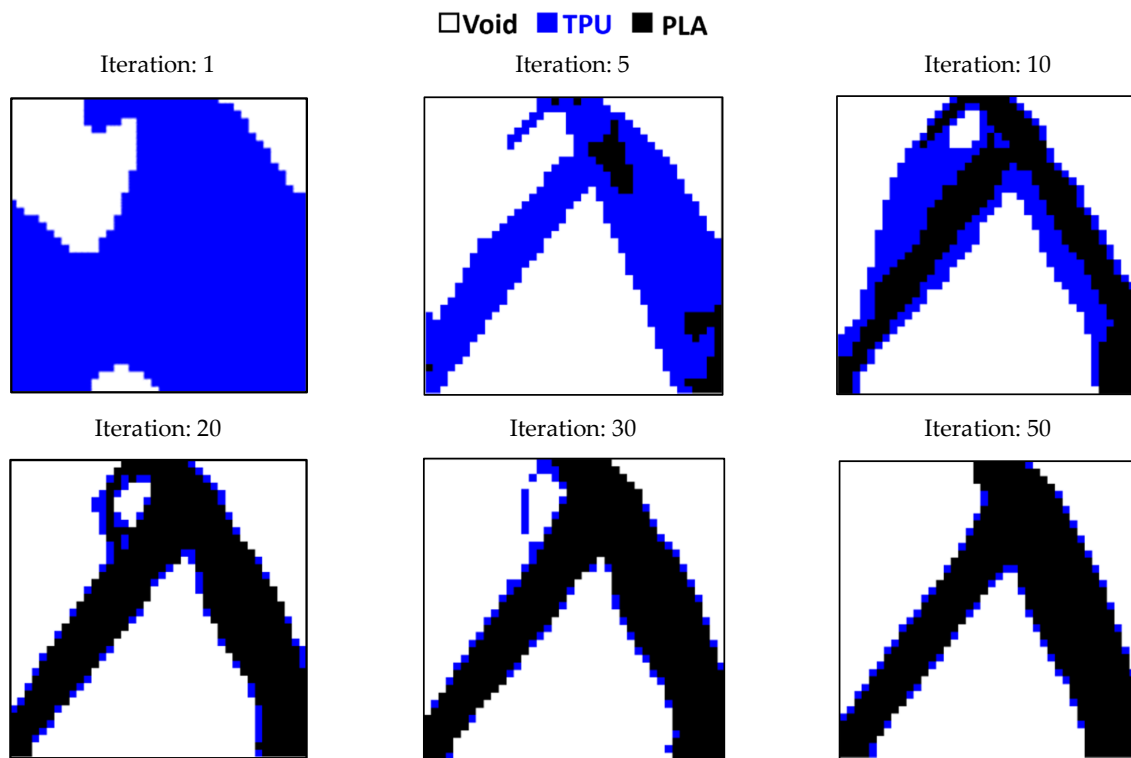


Figure 9. The Optimization of a square plane with multiple materials.

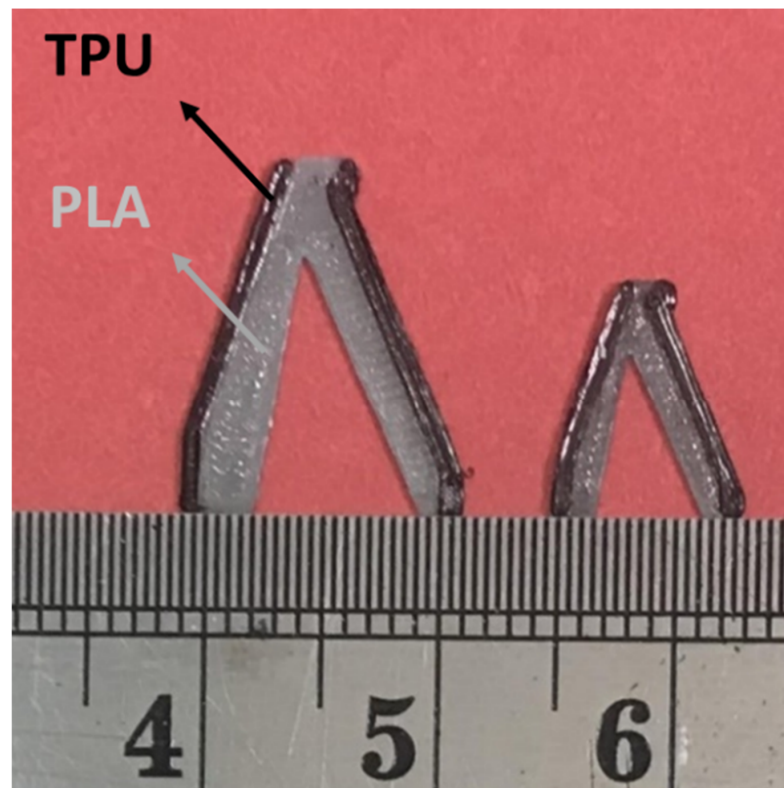


Figure 10. The bi-material metamaterial cells made by FDM 3D printer.

### 3.2. Outputs for Rectangular Plane

In optimization with MATLAB code, a rectangular plane with dimensions of  $4.5 \times 60$  mm is selected. From the rotation of the optimized response, the cylindrical cell is calculated based

on the axisymmetric condition. This cell is radially replaced in the tire. The friction force between the tire and the road leads to bending in this cell. These cells act as a cantilever beam. During the movement and rotation of the tire, bending fatigue loading occurs in these cells. Therefore, the cell can be directly tested for fatigue. In the fatigue test, the sample is connected to the device with a screw at a distance of 1 cm from the beginning and the end. Therefore, this distance from the sample is assumed to be fixed (frozen area).

Since the length of the element is 25 mm, the dimensions of the plane in question were analyzed in a scaled manner. A total of 160 elements along the longitudinal axis and 18 elements along the transverse axis were selected (scale 100 times). Figure 11 shows the results of optimization in different constraints for this plane.



**Figure 11.** The results for the optimization of the rectangular plane in terms of (a) 20%, (b) 40%, and (c) 60% for the weight constraint.

According to this figure, the sample with a residual weight limit of less than 20% had a discontinuity. The sample with a remaining weight of less than 40% cannot be manufactured with the FDM 3D printer due to the creation of very thin struts. Therefore, the sample with a 60% restriction was selected as the optimal sample.

The comparison of the results of the ABAQUS software and MATLAB code with the condition of remaining weight less than 60% is shown in Figure 12. This geometry is also optimized with multiple materials using the MATLAB code and the convergence results of its objective function are illustrated in Figure 13 and the response in a different step of the solution is depicted in Figure 14.

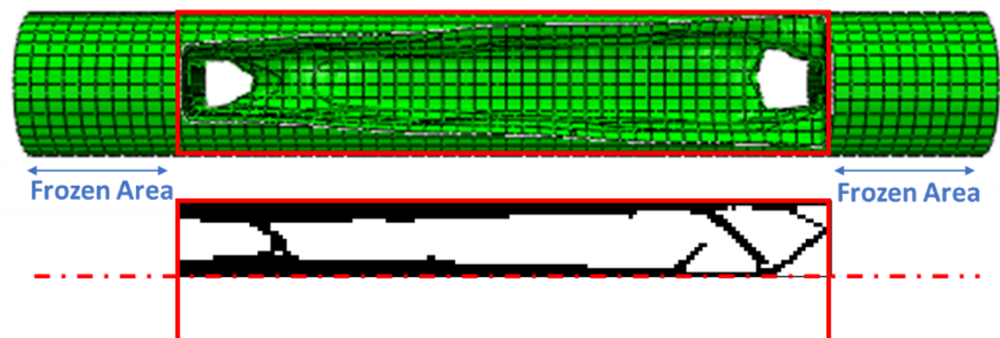


**Figure 12.** The comparison of the results obtained from ABAQUS software and MATLAB code for the rectangular plane. (Note: The red dotted line is the axisymmetric line for the sample).

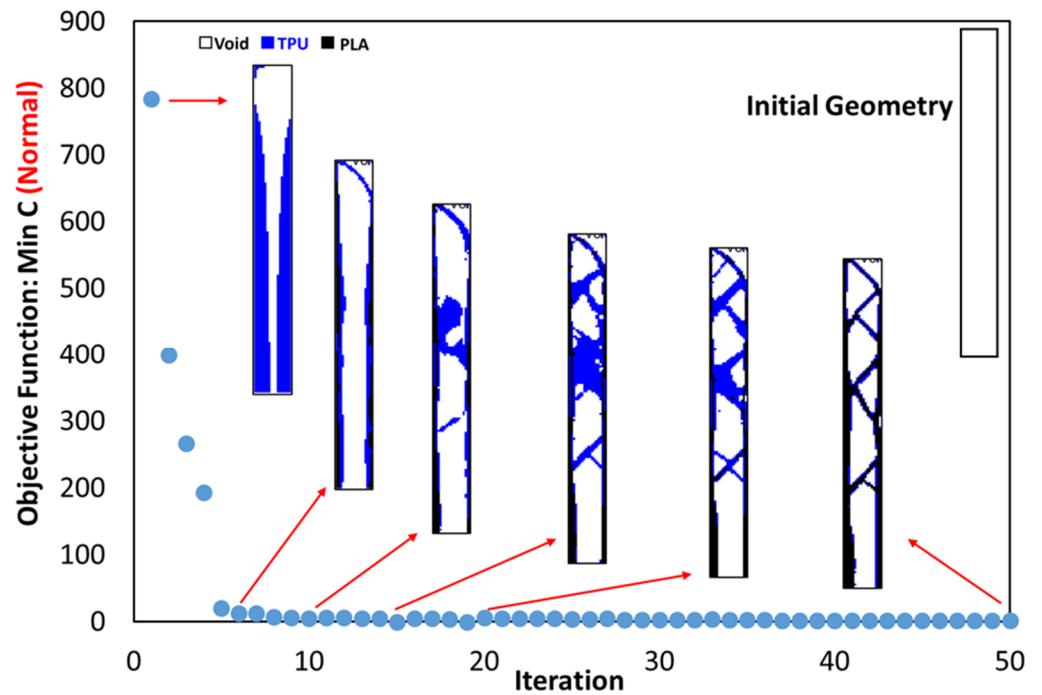


Figure 13. The convergence diagram of objective function for rectangular plane.

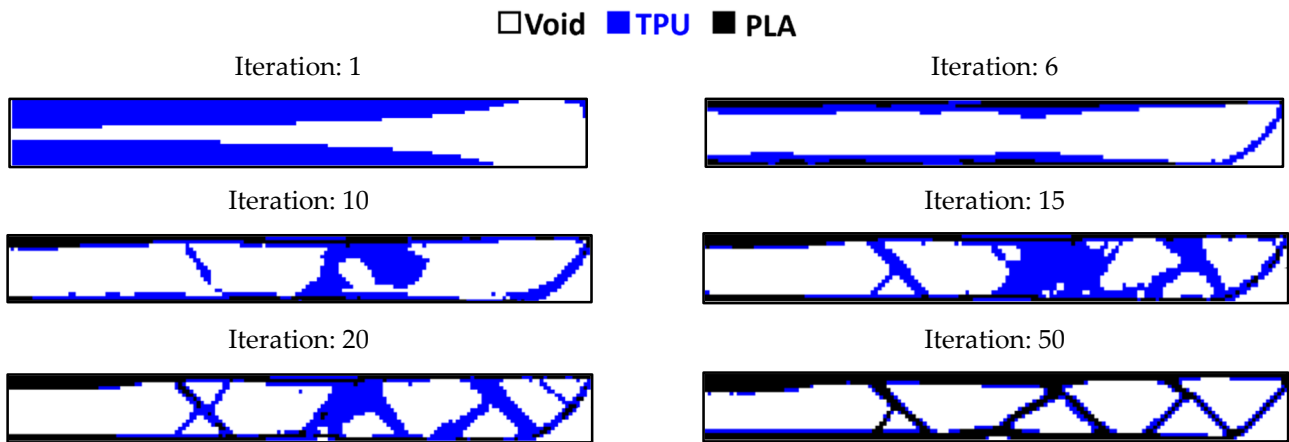


Figure 14. Optimizing the rectangular plane with multiple materials.

### 3.3. Entire Circumference of Tire

This code was also used to optimize the entire circumference of the tire. For this purpose, a square plane with dimensions of  $650 \times 650$  mm was subjected to compressive and bending forces of 5 kN, similar to a real tire. According to the element size, 26 elements were selected in two directions. Figure 15 shows the results of tire optimization with one type of material. Due to this shape, the tire does not have continuity when weight limits of 20% and 40% are used for optimization process. Therefore, taking into account the lowest weight, the tire with 60% was selected as the optimal tire. The same objective function and constraint was used for the optimal distribution of PLA and TPU materials in the tire. The objective function convergence for the tire is shown in Figure 16 and the results are depicted in Figure 17.

Jang et al. [70] also performed topology optimization for tires with the objective function of static stiffness in terms of weight and volume constraints under pressure and tension, separately. The defined supports and tire dimensions were the same as in this study. However, since the optimization of the material distribution was not considered

in the literature [70], the middle part of the tire, which included the tire core, was not considered. In other words, a hole was included in the tire (the inner rim) from the very beginning. Under an optimization formulation, several different patterns were obtained depending on the number of sections, volume fraction, and weighting factors. Among them, three representative patterns were chosen and analyzed for possible applications under working conditions. The value of the objective function in these cells was between 15 and 20 mm/N and the final answer was converged in the number of repetitions between 15 and 30. In contrast, in the current research, the value of the target function was 12 mm/N and the final response was calculated in the number of repetitions of 5.

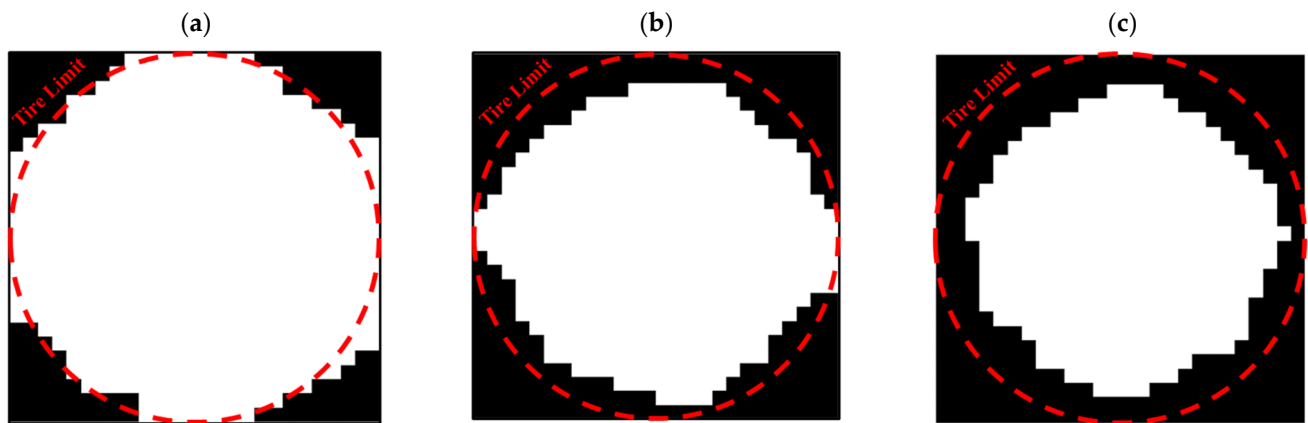


Figure 15. The optimized tire with one type of material: (a) 20%, (b) 40%, and (c) 60% of the weight constraint.

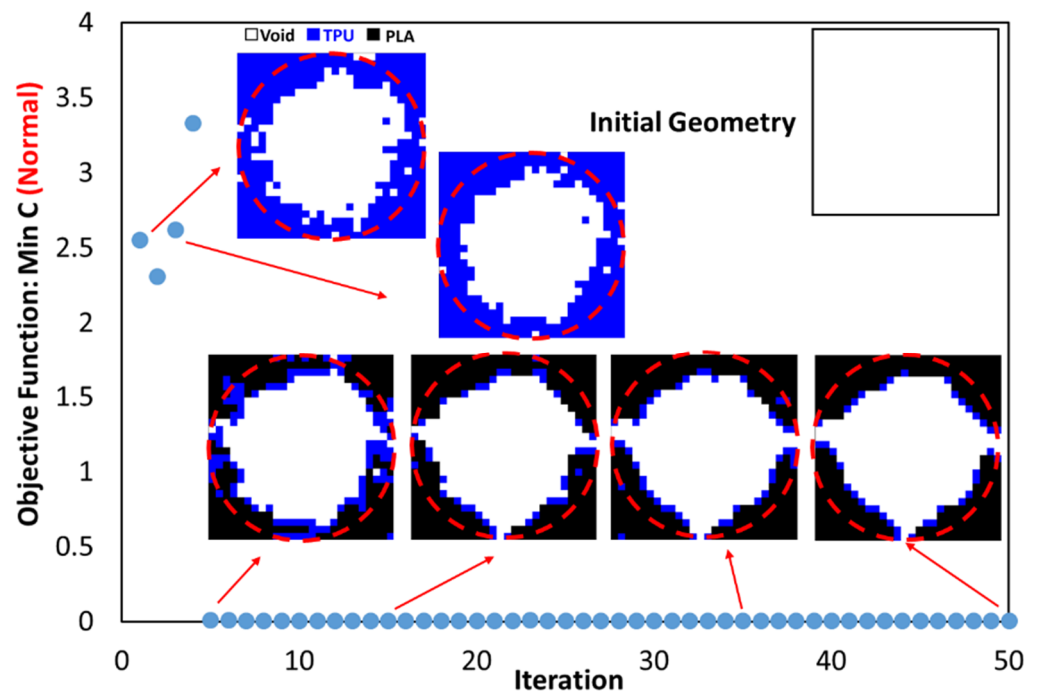
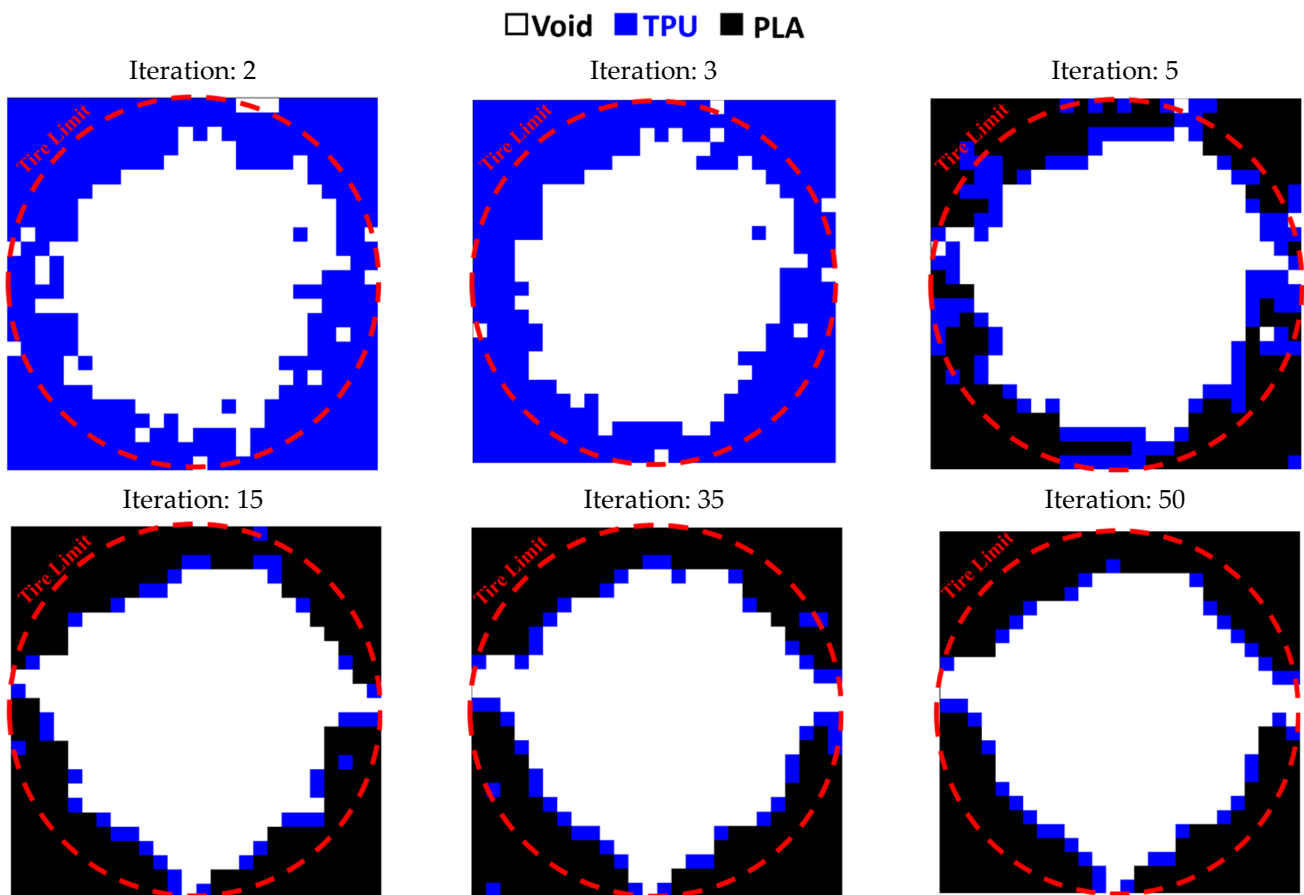


Figure 16. The convergence diagram of the objective function in tire optimization.



**Figure 17.** The results of the optimal distribution of materials in the tire.

This code was also used to optimize a rectangular plane [69]. After optimization, this plane became a semicircle. In addition to optimizing the distribution of two materials, they also implemented the optimization of the distribution of three materials with voids. In the optimization of two materials along with the void, the response was converged in the number of repetitions of 20. The reason for this could be the size of the element used. In this research, the element size was 8 mm. However, in the current research, the size of the element was 25 mm. This smaller element reduced the speed of convergence. In the code, a price value is also included, but the effect of this was not considered in the present study. In addition, 2D and 3D optimizations of a rectangular plane with 1 to 10 materials were implemented [71]. The objective function in these optimizations was the minimum compliance and volume constraint. This plane was subjected to various forces, including tensile and bending, in a 2D state.

In the 2D plane under bending load and two materials, the objective function converged in the number of repetitions of 10. This behavior is similar to the present work. Curved surfaces were also observed in the final response. The percentage of the final volume fraction was 35% to 60%, which is the same as the range of optimized percentages in the current research.

### 3.4. Outputs for The Quality of 3D Printing

The optimized cell of the square plane was fabricated in two sizes of 8 and 10 mm with a 3D FDM printer. Figure 18 shows the image obtained from the FE-SEM of the surface of these two cells. According to this figure, the mechanical adhesion between the PLA and TPU material is quite clear in both scales.

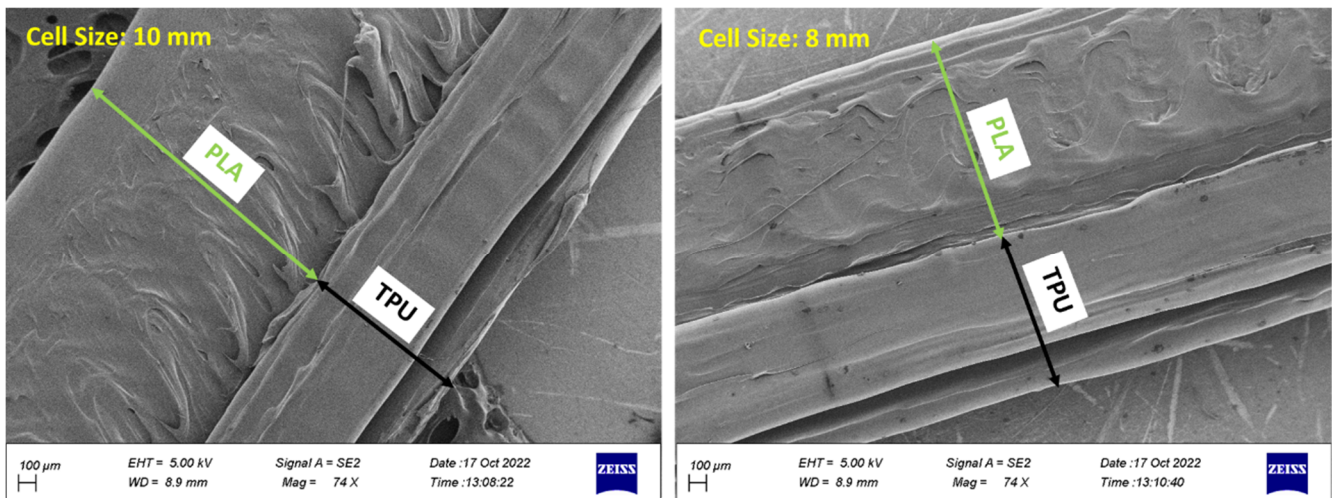


**Figure 18.** The FE-SEM image for connecting PLA/TPU materials.

Holes were observed on the surface of the cells according to Figure 19. These holes are caused by two factors. The first is the high temperature during 3D printing, which causes the filament to evaporate and create bubbles on the surface of the sample. These bubbles cause defects [72]. The second factor is the manufacturing method. In 3D printing, parts are fabricated layer by layer. The improper connection of layers with each other causes holes in the sample. The holes caused by the manufacturing method were observed in connecting similar layers (TPU-TPU) and connecting different layers (PLA-TPU). In addition, the weak connection between layers in the FDM method was observed [72–74]. These holes can be minimized by using optimal print parameters, such as the layer height, the number of shells, and especially the extruder temperature [75].

According to Figure 20, the 3D printed cell with a size of 10 mm was of better quality. In the 3D printed cell with a size of 8 mm, the PLA layers were not well connected to the TPU layer. Various factors affect the adhesion of layers of different materials. Among others, these include print temperature, speed, and density [76,77]. However, these parameters are the same in both sizes. Therefore, it can be concluded that cell size also affects the adhesion of different materials in 3D printing. In other research, it was shown that the large-sized printed sample was of better quality [74].

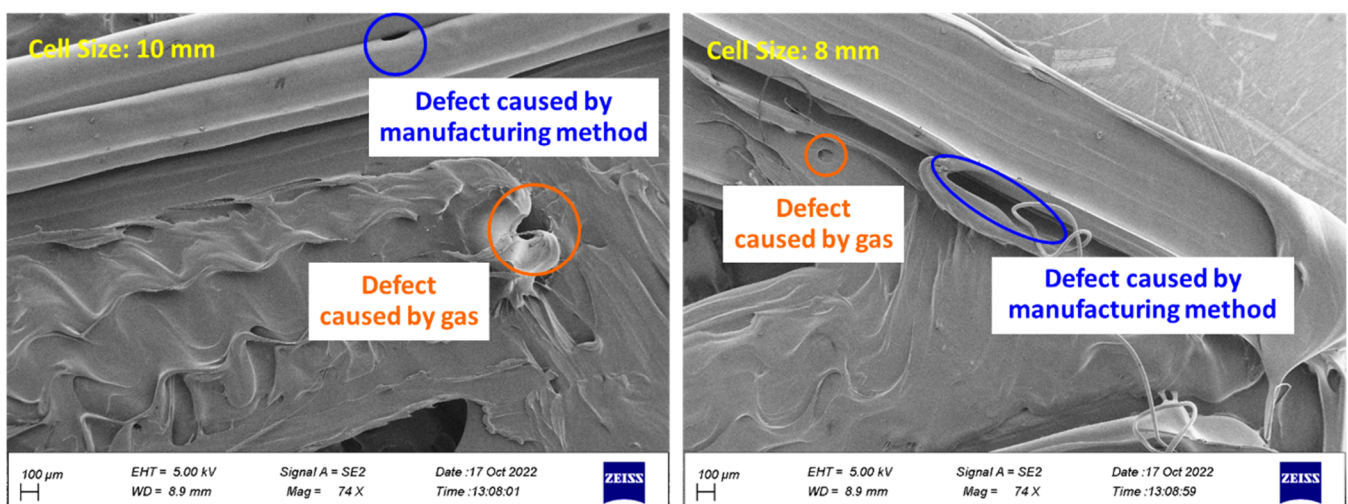


**Figure 19.** The defects fabricated on the surface of the sample during 3D printing.

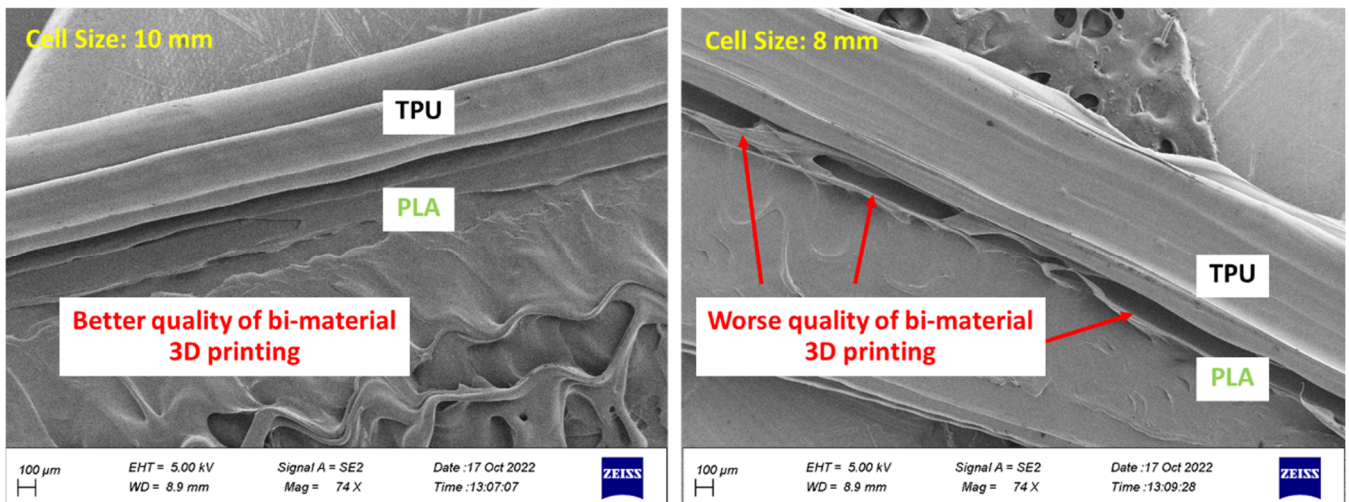


Figure 20. The effect of cell size on the adhesion of two PLA/TPU layers.

Figure 21 shows the cell placement in the tire. In future research, the mechanical properties of this tire will be discussed. When force is applied to this non-pneumatic tire, the adjacent cell structures also have a strong effect on each other, which can affect the structural stress change. In further investigations, the mechanical properties of this tire including compressive and fatigue properties will be discussed. In addition, different arrangements in the unit cell will also be studied.

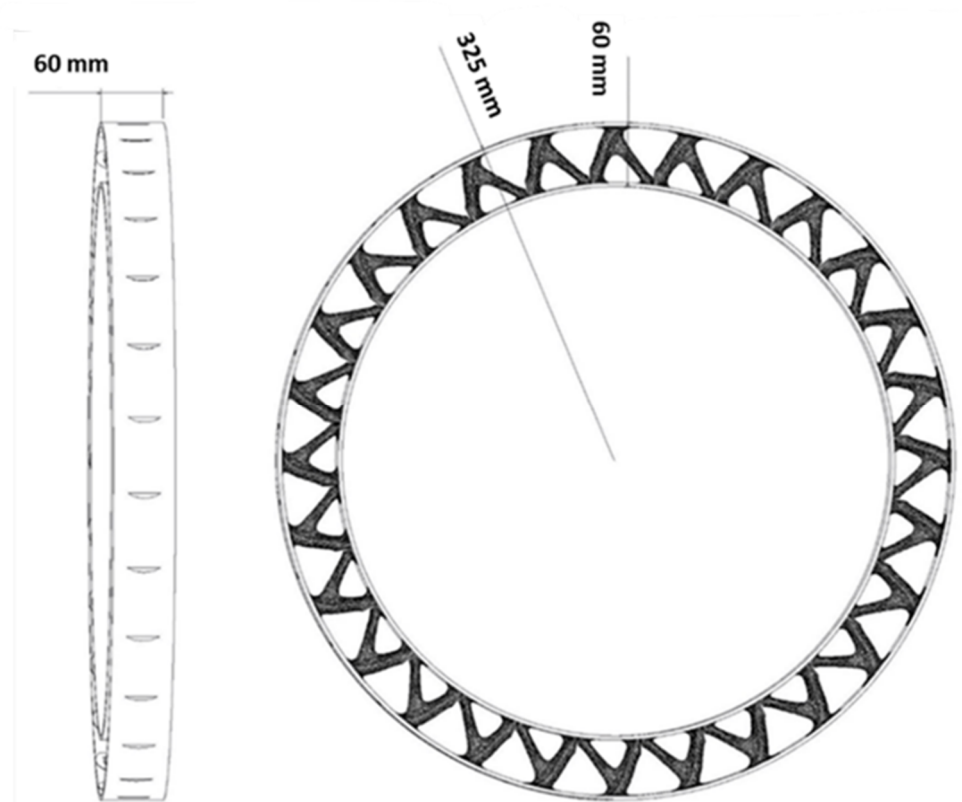


Figure 21. Arrangements of cells in the non-pneumatic tire.

#### 4. Conclusions

In this research, to design a non-pneumatic tire optimization was carried out for three types of geometries, including a square plane, a rectangular plane, and the entire

circumference of the tire, and also using three materials: PLA, TPU, and void. The objective function in this optimization was minimum compliance and weight was a constraint. The results obtained were listed as follows:

- In the optimization of the square plane, the sample with the remaining weight constraint equal to 40% was selected as the optimal sample;
- In the optimization of the rectangular plane, the sample with the remaining weight constraint equal to 60% was selected as the optimal sample;
- In the optimization of the entire circumference of the tire, the sample with a remaining weight of less than 60% was selected as the optimal sample;
- The objective function for all three problems in the optimal distribution of materials was convergent and acceptable;
- PLA and TPU materials had complete mechanical adhesion, based on FE-SEM images. In future research, a pull-off test could be carried out to check this adhesion more accurately.

**Author Contributions:** Conceptualization, M.A.; methodology, M.A.; software, S.D.; validation, M.A.; formal analysis, S.D.; investigation, S.D. and M.A.; resources, S.D. and M.A.; data curation, S.D.; writing—original draft preparation, S.D.; writing—review and editing, M.A.; visualization, M.A.; supervision, M.A.; project administration, M.A.; funding acquisition, M.A. All authors have read and agreed to the published version of the manuscript.

**Funding:** This research was funded by Iran National Science Foundation (INSF), grant number 4002601.

**Institutional Review Board Statement:** Not applicable for studies not involving humans or animals.

**Data Availability Statement:** The data that support the findings of this study are available based on the request from the corresponding author. The experimental data are not publicly available due to restrictions and the privacy of research participants.

**Conflicts of Interest:** The authors declare no conflict of interest. The funders had no role in the design of the study; in the collection, analyses, or interpretation of data; in the writing of the manuscript; or in the decision to publish the results.

## Appendix A

Topology optimization is defined as making macroscopic changes between one or more materials. One of the materials can be considered void. In other words, in topology optimization, by defining the appropriate objective function and constraints, the material distribution in the specimen is optimized. In this method, the specimen is divided into elements and the density of the material is defined as a design variable. Then the properties of the elements are calculated. Some elements are removed and some take the properties of the material. Figure A1a shows a schematic of the solution to the problem in a discrete design. In this design, each color corresponds to a material. The design variable in discrete design can be 0 or 1.

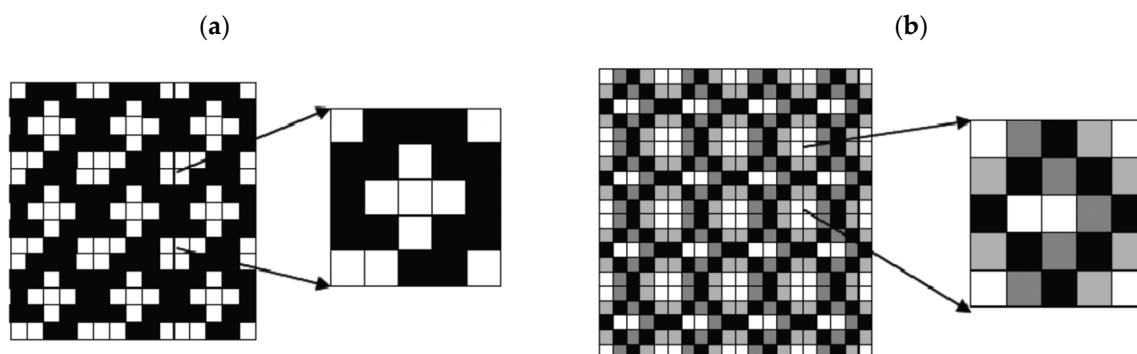


**Figure A1.** The topology optimization including (a) discrete design and (b) continuous design (Note: the white color is *Material 1* and the black one is *Material 2*.) [62].

The optimization problem in the discrete design is defined according to Equation (A1), as follows [62],

$$\begin{aligned}
 &Min : \Phi (C (\rho)) \\
 &s.t. : \sum_{e=1}^N \frac{v_e \rho_e}{v_0} \leq f \\
 &: g_i(C (\rho)) < g_i^* , i = 1, \dots, M \\
 &: \rho_e = \begin{cases} 0 & (\text{material 1}) \\ 1 & (\text{material 2}) \end{cases} , e = 1, \dots, N \\
 &: K(\rho)U_i = F_i , i = 1, \dots, m
 \end{aligned} \tag{A1}$$

In this equation, minimizing  $\Phi$  is the goal of the problem, which includes  $C$ , which is a function of the variable of the problem design and is calculated according to Equation (A2).  $C$  is an interpolation function that determines the properties of each element. These properties can express different physical values such as material stiffness, cost, etc.  $v_e$  is volume of the element,  $(v_0)$  is the unit cell total volume,  $f$  is the volume fraction limit,  $g_i(C (\rho))$  is the problem limit and  $g_i^*$  is the limit. The relationship of  $K(\rho)U_i = F_i$  also represents the finite element analysis for loading cases.

$$C(\rho) = (1 - \rho_e) C^1 + \rho_e C^2 \tag{A2}$$

In this equation,  $C^2$  and  $C^1$  are the material tensors of the two components. If  $\rho_e = 0$ , the element of the properties of the first material is taken, and if  $\rho_e = 1$ , the element of the properties of the second material is taken, and thus a discrete design is obtained. This design brings problems such as creating a design and geometric details that are very delicate and unmanufacturable. One of the ways to solve this problem is to use geometric constraints. In addition, the use of continuous variables is also suggested. In this method, design variables include any value between 0 and 1. As a result, the discrete optimization problem becomes a continuous problem according to Figure A1b. This method is called the gray scheme [63].

In continuous mode, the optimization problem is defined according to Equation (A3) [62].

$$\begin{aligned}
 &Min : \Phi (C (\rho)) \\
 &s.t. : \sum_{e=1}^N \frac{v_e \rho_e}{v_0} \leq f \\
 &: g_i(C (\rho)) < g_i^* , i = 1, \dots, M \\
 &: 0 \leq \rho_e \leq 1 , e = 1, \dots, N \\
 &: K(\rho)U_i = F_i , i = 1, \dots, m
 \end{aligned} \tag{A3}$$

In this method, there is a possibility that the answers will end up in the middle values of the design variables. Therefore, to avoid this problem, different penalty plans are used. For example, it is possible to use the Solid Isotropic Material with a Penalization (SIMP) approach, where the design variable reaches the power of the penalty factor ( $p > 1$ ) and directs the solution toward the discrete values 0 and 1. In fact, despite continuous variables, it performs discrete solutions. In this case, the interpolator function is defined as Equation (A4).

$$C(\rho) = (1 - \rho_e)^p C^1 + \rho_e^p C^2 \tag{A4}$$

If the optimization of only one material is considered, the above relation can be replaced with Equation (A5) [64].

$$C(\rho) = \rho_e^p C^1 \tag{A5}$$

This relationship is used when one of the two materials in question is void. If the optimization of two types of materials with the void is considered, Equation (A6) is used [65].

$$C(\rho) = \rho_e^p \left[ (1 - \rho_e)^p C^1 + \rho_e^p C^2 \right] \tag{A6}$$

Equation (A4) can be extended to three materials [66]:

$$\begin{aligned}
 C^{(1,2,3)}(\rho^1, \rho^2) &= (1 - \rho^1)^p C^1 + (\rho^1)^p C^{2,3} \\
 &= (1 - \rho^1)^p C^1 + (\rho^1)^p [(1 - \rho^2)^p C^2 + \rho^{2p} C^3] \\
 &= (1 - \rho^1)^p C^1 + (\rho^1)^p (1 - \rho^2)^p C^2 + (\rho^1 \rho^2)^p C^3
 \end{aligned}
 \tag{A7}$$

In recent years, another interpolator function according to Equation (A8) has been used, called the modified SIMP method. In this method, the elastic modulus of the cavity is not considered zero to avoid the singularity of the stiffness matrix. One of the advantages of this method is that the elastic modulus and the penalty number are not dependent on each other. In this regard,  $c_{min}$  is the elastic modulus of the cavity [67].

$$C(\rho) = C_{min} + \rho^p (C_0 - C_{min}) \tag{A8}$$

If the interpolator function  $C$  is related to the stiffness of the material, it depends on the elastic modulus and Poisson ratio of the material. In the case that the Poisson ratio is independent of the material density and this tensor is supposed to correspond to a composite material made of empty space and the given material with real density, the bulk modulus ( $K$ ) and the shear modulus ( $\mu$ ) of the tensor ( $C$ ) should cover the Hashin-Shtrikman range.

For two-phase materials, one phase of which is void, the range is shown in Equation (A9) [64].

$$\begin{aligned}
 0 \leq K &\leq \frac{\rho K^0 \mu^0}{(1-\rho)K^0 + \mu^0} \\
 0 \leq \mu &\leq \frac{\rho K^0 \mu^0}{(1-\rho)(K^0 + 2\mu^0) + K^0}
 \end{aligned}
 \tag{A9}$$

In this regard,  $K^0$  and  $\mu^0$  are the bulk modulus and shear modulus of the material in question. In this case, Equation (A10) is calculated for the elastic modulus.

$$0 \leq E \leq \frac{\rho E^0}{3 - 2\rho} \tag{A10}$$

According to Equation (A5), we can say:

$$0 \leq \rho^p E^0 \leq \frac{\rho E^0}{3 - 2\rho} \tag{A11}$$

Equation (A11) is true if, and only if,  $p$  is greater than 3. However, in the SIMP model, the Poisson ratio is assumed to be independent of density. In this case, according to the definitions of the elastic modulus and shear modulus shown in Equation (A12), the Hashin-Shtrikman range is rewritten as Equation (A13):

$$\begin{aligned}
 K &= \frac{E}{2(1-\nu)} \\
 \mu &= \frac{E}{2(1+\nu)}
 \end{aligned}
 \tag{A12}$$

$$\begin{aligned}
 0 \leq \frac{\rho^p E^0}{2(1-\nu)} &\leq \frac{\rho E^0}{4 - 2(1+\nu)\rho} \\
 0 \leq \frac{\rho^p E^0}{2(1+\nu)} &\leq \frac{\rho E^0}{2(1-\rho)(3-\nu) + 2(1+\nu)}
 \end{aligned}
 \tag{A13}$$

From the above relationship, a condition for calculating the value of  $p$  according to Equation (A14) is obtained.

$$p \geq \max\left(\frac{2}{1-\nu}, \frac{4}{1+\nu}\right) \tag{A14}$$

For example, the  $p$  factor for materials with different Poisson ratios is shown in Equation (A15).

$$\begin{aligned} \text{if } \nu &= \frac{1}{3}, p = 3 \\ \text{if } \nu &= \frac{1}{2}, p = 4 \end{aligned} \quad (\text{A15})$$

In the 3D case, the Hashin-Shtrikman range leads to Equation (A16):

$$p \geq \max\left(15 \frac{1-\nu}{7-5\nu}, \frac{3}{2} \frac{1-\nu}{1-2\nu}\right) \quad (\text{A16})$$

In this case, for example, the number  $p$  is calculated as follows:

$$\begin{aligned} \text{if } \nu &= \frac{1}{3}, p \geq 3 \\ \text{if } \nu &= \frac{1}{5}, p \geq 2 \end{aligned} \quad (\text{A17})$$

In general, the larger the  $p$  number, the better it is to remove average densities. However, the solution time increases [68]. Considering that the Poisson's ratio for the materials used in this research is 1/3, therefore, the penalty number of 3 is also considered in the analyses carried out in this research.

In the optimization process, the impact of each design variable on the final response is important. For this reason, sensitivity analysis is performed to find out which variable has the greatest effect on the response. In sensitivity analysis, the effect of that parameter is calculated with the derivative of the desired parameter with respect to the design variable. The higher importance of a parameter causes the solution to have more changes depending on the input variables.

## References

1. Askari, M.; Hutchins, D.A.; Thomas, P.J.; Astolfi, L.; Watson, R.L.; Abdi, M.; Ricci, M.; Laureti, S.; Nie, L.; Freear, S.; et al. Additive manufacturing of metamaterials: A review. *Addit. Manuf.* **2020**, *36*, 101562. [[CrossRef](#)]
2. Refai, K.; Brugger, C.; Montemurro, M.; Saintier, N. An experimental and numerical study of the high cycle multiaxial fatigue strength of titanium lattice structures produced by Selective Laser Melting. *Int. J. Fatigue* **2020**, *138*, 105623. [[CrossRef](#)]
3. Benedetti, M.; du Plessis, A.; Ritchie, R.O.; Dallago, M.; Razavi, S.M.J.; Berto, F. Architected cellular materials: A review on their mechanical properties towards fatigue-tolerant design and fabrication. *Mater. Sci. Eng. R Rep.* **2021**, *144*, 100606. [[CrossRef](#)]
4. Jia, Z.; Liu, F.; Jiang, X.; Wang, L. Engineering lattice metamaterials for extreme property, programmability, and multifunctionality. *J. Appl. Phys.* **2020**, *127*, 150901. [[CrossRef](#)]
5. Frenzel, T.; Kadic, M.; Wegener, M. Three-dimensional mechanical metamaterials with a twist. *Science* **2017**, *358*, 1072–1074. [[CrossRef](#)]
6. Deptula, A.; Osinski, P. The Optimization of Three-Involute Tooth Outline with Taking into Consideration Multi-valued Logic Trees. In Proceedings of the 13th International Scientific Conference: Computer Aided Engineering, Wroclaw, Poland, 22–24 June 2016.
7. Jafferson, J.M.; Sharma, H. Design of 3D printable airless tyres using NTopology. *Mater. Today: Proc.* **2021**, *46*, 1147–1160. [[CrossRef](#)]
8. Sandberg, U. The airless tire: Will this revolutionary concept be the tire of the future? *Mod. Concepts Mater. Sci.* **2020**, *3*, 000563. [[CrossRef](#)]
9. Bras, B.; Cobert, A. Life-cycle environmental impact of Michelin tweel<sup>®</sup> tire for passenger vehicles. *SAE Int. J. Passeng. Cars Mech. Syst.* **2011**, *4*, 32–43. [[CrossRef](#)]
10. Sambucci, M.; Valente, M. Ground waste tire rubber as a total replacement of natural aggregates in concrete mixes: Application for lightweight paving blocks. *Materials* **2021**, *14*, 7493. [[CrossRef](#)]
11. Shinichi, S.; Hideto, Y.; Yasuhiro, H.; Misuzu, A.; Hidetaka, T.; Shin, T.; Keijirou, T.; Maria Victoria, P.; Jakub, W.; Douvan, T.; et al. International comparative study of 3R and waste management policy developments. *J. Mater. Cycles Waste Manag.* **2011**, *13*, 86–102.
12. Jin, X.; Hou, C.; Fan, X.; Sun, Y.; Lv, J.; Lu, C. Investigation on the static and dynamic behaviors of non-pneumatic tires with honeycomb spokes. *Compos. Struct.* **2018**, *187*, 27–35. [[CrossRef](#)]
13. Mazur, V.V. Experiments to find the rolling resistance of non-pneumatic tires car wheels. In Proceedings of the 5th International Conference on Industrial Engineering, Sochi, Russia, 25–29 March 2019; pp. 641–648.
14. Deziania, S.; Azadi, M. A review on metamaterial types, additive manufacturing technique and its application in automotive industry. *Sci. J. Iran. Soc. Mech. Eng.* **2021**, *4*, 70–80.

15. Suvanjumrat, C.; Rugsaj, R. Study of 3D printing for forming spoke of non-pneumatic tire using finite element method. *IOP Conf. Ser. Mater. Sci. Eng.* **2021**, *1137*, 012020. [[CrossRef](#)]
16. Rugsaj, R.; Suvanjumrat, C. Dynamic finite element analysis of rolling non-pneumatic tire. *Int. J. Automot. Technol.* **2021**, *22*, 1022. [[CrossRef](#)]
17. Rugsaj, R.; Suvanjumrat, C. Determination of material property for non-pneumatic tire spokes by inverse method. *Key Eng. Mater.* **2018**, *777*, 411–415. [[CrossRef](#)]
18. Rugsaj, R.; Suvanjumrat, C. Proper radial spokes of non-pneumatic tire for vertical load supporting by finite element analysis. *Int. J. Automot. Technol.* **2019**, *20*, 801–812. [[CrossRef](#)]
19. Ramachandran, M. Nonlinear Finite Element Analysis of Tweel Geometric Parameter Modifications on Spoke Dynamics During High-Speed Rolling. Master's Thesis, Clemson University, Clemson, SC, USA, 2008.
20. Manibaalan, C.; Keshore, B.S.; Haran, J.C. Static analysis of airless tyres. *Int. J. Sci. Res. Publ.* **2013**, *3*, 1–4.
21. Zmuda, M.; Jackowski, J.; Hryciow, Z. Numerical research of selected features of the non-pneumatic tire. *AIP Conf. Proc.* **2019**, *2078*, 020027.
22. Ma, J.; Summers, J.; Joseph, P. Dynamic impact simulation of interaction between non-pneumatic tire and sand with obstacle. In Proceedings of the SAE 2011 World Congress and Exhibition, Detroit, MI, USA, 12–14 April 2011; Volume 12.
23. Ma, J.; Summers, J.D.; Joseph, P.F. Numerical simulation of tread effects on the interaction between cellular shear band based non-pneumatic tire and sand. In Proceedings of the ASME Design Engineering Technical Conference, Washington, DC, USA, 28–31 August 2011; Volume 8, pp. 769–779.
24. Shankar, P.; Fazelpour, M.; Summers, J.D. An energy-based design approach for a meso-structure with high shear flexure. In Proceedings of the ASME Design Engineering Technical Conference, Portland, OR, USA, 4–7 August 2013; Volume 3.
25. Ma, J.; Louis, S.; Summers, J.D.; Joseph, P.F. Numerical Investigation of Effect of Membrane on Thickness on the Performance of Cellular Shear Band Based non-pneumatic Tire. In Proceedings of the International Design Engineering Technical Conferences and Computers and Information in Engineering Conference, Washington, DC, USA, 28–31 August 2011; pp. 1–11.
26. Tavakoli, R. Multimaterial topology optimization by volume constrained Allen–Cahn system and regularized projected steepest descent method. *Comput. Methods Appl. Mech. Eng.* **2014**, *276*, 534–565. [[CrossRef](#)]
27. Han, Z.; Gu, Z.; Ma, X.; Chen, W. Multi material layout optimization of truss structures via an improved particle swarm optimization algorithm. *Comput. Struct.* **2019**, *222*, 10–24.
28. Chen, Y.; Ye, L.; Xu, C.; Zhang, Y.X. Multi-material topology optimization of micro-composites with reduced stress concentration for optimal functional performance. *Mater. Des.* **2021**, *210*, 110098. [[CrossRef](#)]
29. Chung, H.; Du, Z. Optimized design of multi-material cellular structures by a level-set method with Guyan reduction. *J. Mech. Des.* **2021**, *143*, 101702. [[CrossRef](#)]
30. Mansouri, M.R.; Montazerian, H.; Schmauder, S. 3D-printed multi-material composites tailored for compliancy and strain recovery. *Compos. Struct.* **2018**, *184*, 11–17. [[CrossRef](#)]
31. Gao, X.; Caivano, R.; Tridello, A.; Chiandussi, G.; Ma, H.; Paolino, D.; Berto, F. Innovative formulation for topological fatigue optimization based on material defects distribution and TopFat algorithm. *Int. J. Fatigue* **2021**, *17*, 106176. [[CrossRef](#)]
32. Gao, J.; Wang, L.; Xiao, M.; Gao, L.; Li, P. An ISO geometric approach to topological optimization design of auxetic composites with tri-material micro-architectures. *Compos. Struct.* **2021**, *271*, 114163. [[CrossRef](#)]
33. Huang, X.; Li, W. A new multi-material topology optimization algorithm and selection of candidate materials. *Comput. Methods Appl. Mech. Eng.* **2021**, *386*, 114114. [[CrossRef](#)]
34. Li, H.; Luo, Z.; Gao, L.; Walker, P. Topology optimization for functionally graded cellular composites with metamaterials by level sets. *Comput. Methods Appl. Mech. Eng.* **2018**, *328*, 340–364. [[CrossRef](#)]
35. Nguyen, C.; Zhuang, X.; Chamoin, L.; Zhao, X.; Nguyen-Xuan, H.; Rabczuk, T. Three-dimensional topology optimization of auxetic metamaterial using isogeometric analysis and model order reduction. *Comput. Methods Appl. Mech. Eng.* **2020**, *371*, 113306. [[CrossRef](#)]
36. Vogiatzis, P.; Chen, S.; Wang, X.; Li, T.; Wang, L. Topology optimization of multi-material negative Poisson's ratio metamaterials using a reconciled level set method. *Comput. Aided Des.* **2017**, *83*, 15–32. [[CrossRef](#)]
37. Huikai, Z.; Yangjun, L.; Kang, Z. Bi-material microstructural design of chiral auxetic metamaterials using topology optimization. *Compos. Struct.* **2018**, *195*, 232–248.
38. Zheng, Y.; Wang, Y.; Lu, X.; Zheng, J.; Qu, J. Topology optimization for isotropic mechanical metamaterials considering material uncertainties. *Mech. Mater.* **2021**, *155*, 103742. [[CrossRef](#)]
39. Deng, Y.; Zhao, Y.; Lin, F.; Xiao, Z.; Zhu, M.; Li, H. Simulation of steady-state rolling non-pneumatic mechanical elastic wheel using finite element method. *Simul. Model. Pract. Theory* **2018**, *85*, 60–79. [[CrossRef](#)]
40. Du, X.; Zhao, Y.; Wang, Q.; Fu, H.; Lin, F. Grounding characteristics of a non-pneumatic mechanical elastic tire in a rolling state with a camber angle. *Stroj. Vestn. J. Mech. Eng.* **2019**, *65*, 287–296. [[CrossRef](#)]
41. Du, X.; Zhao, Y.; Lin, F.; Fu, H.; Wang, Q. Numerical and experimental investigation on the camber performance of a non-pneumatic mechanical elastic wheel. *J. Braz. Soc. Mech. Sci. Eng.* **2017**, *39*, 3315–3327. [[CrossRef](#)]
42. Xiao, Z.; Zhao, Y.Q.; Lin, F.; Zhu, M.M.; Deng, Y.J. Studying the fatigue life of a non-pneumatic wheel by using finite-life design for life prediction. *J. Mech. Eng.* **2018**, *64*, 56–67.

43. Zhao, Y.Q.; Xiao, Z.; Lin, F.; Zhu, M.M.; Deng, Y.J. Influence analysis of machining and installation errors on the radial stiffness of a non-pneumatic mechanical elastic wheel. *Chin. J. Mech. Eng.* **2018**, *31*, 1–9. [[CrossRef](#)]
44. Mathew, N.J.; Sahoo, D.K.; Chakravarthy, E.M. Design and static analysis of airless tyre to reduce deformation. *IOP Conference Ser. Mater. Sci. Eng.* **2017**, *197*, 012042. [[CrossRef](#)]
45. Zhang, Z.; Fu, H.; Zhao, Q.; Tan, D.; Yang, K. Pattern design and performance analysis of a flexible spoke bionic non-pneumatic tire. *J. Braz. Soc. Mech. Sci. Eng.* **2021**, *43*, 1–11. [[CrossRef](#)]
46. Zhang, Z.; Fu, H.; Liang, X.; Chen, X.; Tan, D. Comparative analysis of static and dynamic performance of nonpneumatic tire with flexible spoke structure. *Stroj. Vestn. J. Mech. Eng.* **2020**, *66*, 458–466. [[CrossRef](#)]
47. Wang, J.; Yang, B.; Lin, X.; Gao, L.; Liu, T.; Lu, Y.; Wang, R. Research of TPU materials for 3D printing aiming at non-pneumatic tires by FDM method. *Polymers* **2020**, *12*, 2492. [[CrossRef](#)]
48. Ganniari-Papageorgiou, E.; Chatzistergos, P.; Wang, X. The Influence of the honeycomb design parameters on the mechanical behavior of non-pneumatic tires. *Int. J. Appl. Mech.* **2020**, *12*, 2050024. [[CrossRef](#)]
49. Zheng, Z.; Rakheja, S.; Sedaghati, R. Multi-axis stiffness and road contact characteristics of honeycomb wheels: A parametric analysis using Taguchi method. *Compos. Struct.* **2022**, *279*, 114735. [[CrossRef](#)]
50. Fu, H.; Chen, X.; Zhao, Q.; Xiao, Z.; Liang, X. Fatigue life prediction and influencing factors analysis of mesh flexible spoke non-pneumatic tire. *Adv. Mech. Eng.* **2021**, *13*, 1–10. [[CrossRef](#)]
51. Gami, A.; Joseph, P.F.; Rhyne, T.B.; Cron, S.M. Development of a two-dimensional model of a compliant non-pneumatic tire. *Int. J. Solids Struct.* **2012**, *49*, 1723–1740. [[CrossRef](#)]
52. Ju, J.; Kim, D.M.; Kim, K. Flexible cellular solid spokes of a non-pneumatic tire. *Compos. Struct.* **2012**, *94*, 2285–2295. [[CrossRef](#)]
53. Maharaj, Y.; James, K.A. Metamaterial topology optimization of nonpneumatic tires with stress and buckling constraints. *Int. J. Numer. Methods Eng.* **2020**, *121*, 1410–1439. [[CrossRef](#)]
54. Petrone, F.; Fichera, G.; Lacagnina, M. A numerical model to analyze the dynamic response of a vehicle to variations in torque transmitted by the drive-line. *SAE Int. J. Passeng. Cars Mech. Syst.* **2001**, *2*, 2544–2553.
55. Hsiao, T.; Liu, N.; Chen, S. Robust estimation of the friction forces generated by each tire of a vehicle. In Proceedings of the 2011 American Control Conference, San Francisco, CA, USA, 29 June–1 July 2011; pp. 5261–5266.
56. Wei, W.; Kai, Z.; Shaoyi, B.; Lanchun, Z.; Yongzhi, W. Vibration performance analysis of vehicle with the non-pneumatic new mechanical elastic wheel in the impulse input experiment. *J. Vibroengineering* **2016**, *18*, 3970–3980. [[CrossRef](#)]
57. Zhao, Y.; Du, X.; Lin, F.; Wang, Q.; Fu, H. Static stiffness characteristics of a new non-pneumatic tire with different hinge structure and distribution. *J. Mech. Sci. Technol.* **2018**, *32*, 3057–3064. [[CrossRef](#)]
58. Zhao, Y.Q.; Deng, Y.J.; Lin, F.; Zhu, M.M.; Xiao, Z. Transient dynamic characteristics of a non-pneumatic mechanical elastic wheel rolling over a ditch. *Int. J. Automot. Technol.* **2018**, *19*, 499–508. [[CrossRef](#)]
59. Torres, J.; Cotel, J.; Karl, J.; Gordon, A.P. Mechanical property optimization of FDM PLA in shear with multiple objectives. *Miner. Met. Mater. Soc. Mech.* **2015**, *67*, 1183–1193. [[CrossRef](#)]
60. Dezhianian, S. Topology Optimization of the Vehicle Non-Pneumatic Tire from Multi-Material Metamaterial with the Objective of Compressive Strength and Bending Fatigue Lifetime. Master's Thesis, Semnan University, Semnan, Iran, 2022.
61. Schollenberger, C.S.; Stewart, F.D. Thermoplastic Polyurethane Hydrolysis Stability. *J. Elastomers Plast.* **2016**, *3*, 28–56. [[CrossRef](#)]
62. Pyrz, R.; Rauhe, J.C. IUTAM Symposium on Modelling Nanomaterials and Nanosystems. In Proceedings of the IUTAM Symposium, Aalborg, Denmark, 19–22 May 2008; Volume 13.
63. Panesar, A. Review on design and structural optimization in additive manufacturing: Towards next-generation lightweight structures. *Mater. Des.* **2019**, *183*, 108164.
64. Bendsoe, M.P.; Sigmund, O. Material interpolation schemes in topology optimization. *Arch. Appl. Mech.* **1999**, *69*, 635–654. [[CrossRef](#)]
65. Sigmund, O. Design of Multiphysics actuators using topology optimization, Part II: Two-material structures. *Comput. Methods Appl. Mech. Eng.* **2001**, *190*, 6605–6627. [[CrossRef](#)]
66. Li, D.; Yong, I. Multi-material topology optimization for practical lightweight design. *Struct. Multidiscip. Optimization* **2018**, *58*, 1081–1094. [[CrossRef](#)]
67. Liu, K.; Tovar, A. An efficient 3D topology optimization code written in Matlab. *Computer Methods Appl. Mech. Eng.* **2014**, *340*, 798–823. [[CrossRef](#)]
68. Grinde, S.; Tech, M. Topology Optimization for Additive Manufacturing Using SIMP Method. Master's Thesis, Montana Technological University, Butte, MT, USA, 2018.
69. Zuo, W.; Saitou, K. Multi-material topology optimization using ordered SIMP interpolation. *Struct. Multidiscip. Optim.* **2017**, *55*, 477–491. [[CrossRef](#)]
70. Jang, I.G.; Sung, Y.H.; Yoo, E.J.; Kwak, B.M. Pattern design of a non-pneumatic tyre for stiffness using topology optimization. *Eng. Optim.* **2012**, *44*, 119–131. [[CrossRef](#)]
71. Sanders, E.D.; Aguiló, M.A.; Paulino, G.H. Multi-material continuum topology optimization with arbitrary volume and mass constraints. *Comput. Methods Appl. Mech. Eng.* **2018**, *340*, 798–823. [[CrossRef](#)]
72. Azadi, M.; Dadashi, A.; Dezhianian, S.; Kianifar, M.; Torkaman, S.; Chiyani, M. High-cycle bending fatigue properties of additive-manufactured ABS and PLA polymers fabricated by fused deposition modeling 3D-printing. *Forces Mech.* **2021**, *3*, 100016. [[CrossRef](#)]

73. Ning, F.; Cong, W.; Qiu, J.; Wei, J.; Wang, S. Additive manufacturing of carbon fiber reinforced thermoplastic composites using fused deposition modeling. *Compos. Part B Eng.* **2015**, *80*, 369–378. [[CrossRef](#)]
74. Azadi, M.; Dadashi, A.; Aghareb Parast, M.S.; Dezhianian, S. A comparative study for high-cycle bending fatigue lifetime and fracture behavior of extruded and additive-manufactured 3D-printed acrylonitrile butadiene styrene polymers. *Int. J. Addit. Manuf. Struct.* **2022**, *1*, 1.
75. Ferretti, P.; Leon-Cardenas, C.; Santi, G.; Sali, M.; Ciotti, E.; Frizziero, L.; Donnici, G.; Liverani, A. Relationship between FDM 3D Printing Parameters Study: Parameter Optimization for Lower Defects. *Polymers* **2021**, *13*, 2190. [[CrossRef](#)]
76. Yadav, D.; Chhabra, D.; Kumar Garg, R.; Ahlawat, A.; Phogat, A. Optimization of FDM 3D printing process parameters for multi-material using artificial neural network. *Mater. Today Proc.* **2020**, *21*, 1583–1591. [[CrossRef](#)]
77. Yin, J.; Lu, C.; Fu, J.; Huang, Y.; Zheng, Y. Interfacial bonding during multi-material fused deposition modeling (FDM) process due to inter-molecular diffusion. *Mater. Des.* **2018**, *150*, 104–112. [[CrossRef](#)]

**Disclaimer/Publisher’s Note:** The statements, opinions and data contained in all publications are solely those of the individual author(s) and contributor(s) and not of MDPI and/or the editor(s). MDPI and/or the editor(s) disclaim responsibility for any injury to people or property resulting from any ideas, methods, instructions or products referred to in the content.